Self-interference Cancelation Performance in Full-Duplex Jamming and Spectrum Monitoring

Jaakko Marin, Matias Turunen, Micael Bernhardt, and Taneli Riihonen

Electrical Engineering, Tampere University, Finland
e-mail: jaakko.marin@tuni.fi

***Abstract*—The use of drones in illegal activities has increased in recent years. One method for countering their operation in restricted areas is by transmitting a high-powered jamming signal over the frequencies used by the target drone. To improve the performance of jammers, full-duplex is introduced. In full-duplex systems, the transceiver is able to transmit and receive using the same time-frequency resources, which allows a device to conduct spectrum monitoring while preventing drone operations by transmitting jamming. In this study, the self-interference cancelation of typical jamming waveforms is experimentally measured and signal detection is performed over samples with imperfect self-interference cancelation.**

I. Introduction

The rapid increase in the amount of commercial class drones has caused concern because of the potential unlawful use of such devices [1]. While there is a strong push in Europe to register every drone and its user, there will still probably be times when a certain drone needs to be forcibly shut down. While the option of shooting the drone down with nets or bullets might be ill-advised in domestic environments, another effective method to counter drones is the use of jamming [2]. Simply put, jamming refers to sending a strong interference signal to disrupt the reception of the target receiver [3]. Various different waveforms can be used against the protocol utilized by the target communication system [4].

The problem with jamming is that it also affects other users of the radio spectrum, including any devices close to the jammer. Therefore, to minimize the collateral damage to legitimate users, the frequency and time use of jamming should be optimized against the target. Furthermore, observing the behavior of the target system is important in case it moves to different radio or spatial resources as a reaction to being jammed. In a traditional half-duplex system this means that to observe the channel for other users and target behavior, jamming has to be periodically paused. To make this operation more efficient, we propose using a full-duplex capable transceiver.

Full-duplex (FD) refers to using the same time-frequency resources to transmit and receive simultaneously. For effective operation, the received signal transmitted by the own system, or self-interference (SI), needs to be canceled in the reception. The use of FD systems in communication applications has been extensively studied [5], and our department has produced various experiments showing the performance of such a system in different real-world scenarios [6]–[11]. The self-interference cancelation methods and prototype used in this study are the same as in our previous publications.

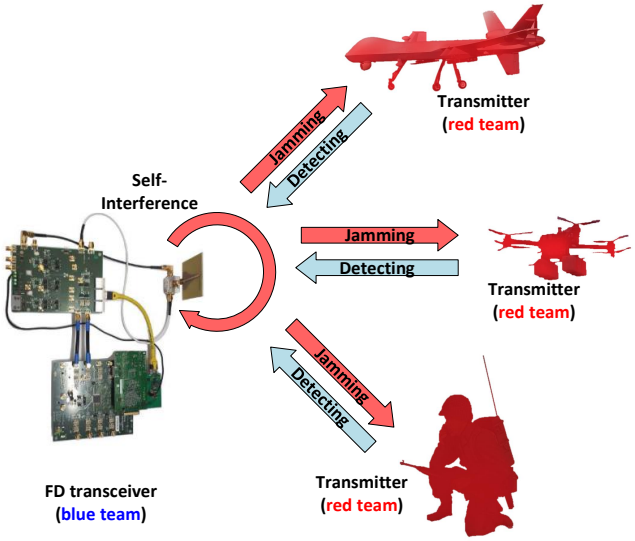

Fig. 1. Sketch of a possible use case. The blue team is simultaneously jamming the communication systems of the red team while detecting their transmissions.

To allow simultaneous jamming and spectral monitoring, a FD capable system should be used. This is especially important, since there exist various methods to counter different jamming waveforms in research literature [12]–[15]. A smart jammer would need to monitor the behavior of the target under jamming and, if necessary, to adapt the transmitted waveform to guarantee successful operation. Such a system can be seen in Fig. 1. In order to ensure spectral monitoring capability, the transceiver needs to be able to effectively cancel all the possible jamming waveforms. To the best of our knowledge, there is no existing public research concerning the SI cancelation performance of FD systems for typical jamming waveforms. This information could help when defending against any malicious RF-systems, not just drones.

This research work was funded by the Finnish Scientific Advisory Board for Defence (MATINE — Maanpuolustuksen tieteellinen neuvottelukunta) under the project 2500M-0117 “Electronic Interception of Unmanned Aerial Vehicles” and the Academy of Finland under the grant 315858 “Radio Shield Against Malign Wireless Communication.”

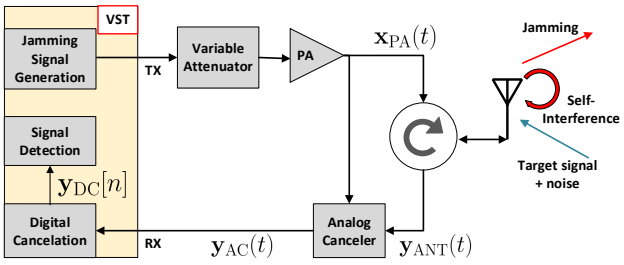

Fig. 2. Block diagram of the experiment setup.

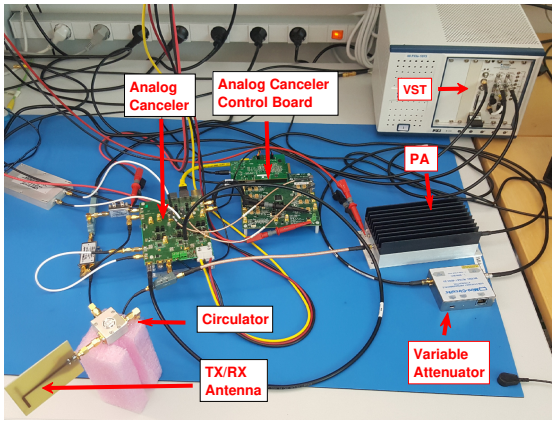

Fig. 3. A photo of our department's prototype full-duplex radio and the measurement system used in this study.

This work is a continuation of our previous publication in [16], where the jamming performance of different waveforms was experimentally studied against a cheap RC receiver. In our current study a FD capable transceiver doing simultaneous jamming and spectral monitoring is developed and the SI cancelation performance with the waveforms used in the previous publication are measured. Additionally, signal detection performance from received samples with imperfect SI cancelation is analyzed.

II. Experimental Setup and Waveforms

During our earlier measurement campaign for a database of drone RF-signal measurements [17], we found that commercial class drones commonly use protocols situated on the shared 2.4 GHz and 5 GHz industrial, medical, and scientific (ISM) bands. Typically, standard WiFi protocols, or the like, are utilized for audiovisual feedback and narrowband frequency hopping (FH) protocols are used for control signaling. Additionally, global navigation satellite systems (GNSS) can be used to determine the location of the drone. Herein we focus on FD canceling performance of jamming waveforms designed against FH control signals.

In our previous study [16], different jamming waveforms were tested against a cheap RC system utilizing AMICCOM A7105 based wireless transceiver chips. This system did not have a video link. The chips used automatic frequency hopping digital system (AFHDS) protocol, where the transmitted signal was a Gaussian frequency-shift keyed (GFSK) signal hopping on 14 subbands with a bandwidth of 500-kHz each, and centered around the 2.4 GHz ISM band. These jamming waveforms were:

- Noise with 80 MHz bandwidth.
- Tone at each of the 14 carrier frequencies of the RC receiver.
- Tones at frequencies defined by the GFSK modulation used by the RC system.
- Tone at the carrier and the GFSK frequencies used by the RC system.
- Noise with 500 kHz bandwidth at every carrier frequency of the RC system.
- Frequency hopping tones at GFSK frequencies used by the RC system. The sweeping frequency was varied.
- Triangular sweep moving through the whole 80 MHz band with varying sweep frequencies.

Refer to [Fig. 1, 16] for illustrations on the spectra of the signals. In this study, we determine how well our FD system is capable of canceling these waveforms. Although these waveforms have only been tested to be effective against the protocol used by the specific RC system examined in the previous study, the chosen waveforms should be effective against commercial drones as well, since most of them use some form of a FH protocol for control signaling [18]. When adapting the jamming waveform against these devices, the exact frequencies of the tones, optimal noise bandwidths and the hopping pattern's carrier frequencies will vary with different target protocols, but the fundamental FD cancelation operation stays the same. Therefore it can be presumed, that from the point of view of cancelation and subsequent signal detection, these exact details are of minor importance.

The experimental FD system and a picture of the completed setup can be seen in Figs. 2 and 3. The system transmits a jamming waveform to interfere with the reception of other channel users. It simultaneously receives the signals from other users, and its own TX signal as SI. The other signals might be several orders of magnitude weaker than the SI, but by effective SI cancelation these signals can be detected.

The transceiver used is a National Instruments PXIe-5645R vector signal transceiver (VST), which both generates the transmitted jamming signal and receives the samples which are then taken to offline processing. The variable attenuator and the power amplifier (PA) are used to control the final signal power at the transmit (TX) antenna. The system operates with a single antenna. The receive (RX) and TX sides are connected with a circulator, where the TX-to-RX isolation is 20 dB.

A. Self-interference Cancelation

The received signal from the RX port of the circulator can be expressed with

$$y_{\mathrm{ANT}}(t) = h(t) * x_{\mathrm{PA}}(t) + \sum_{i=1}^{K} s_i(t) + z(t), \qquad (1)$$

where $h(t)$ is the multipath channel experienced by the transmit signal $x_{\mathrm{PA}}(t)$, $z(t)$ is additive thermal noise, $s_i(t)$ is a signal of user i and K is the total number of other users of the channel — $s_i(t)$ and K are assumed to be totally unknown.

The analog canceler takes the transmit signal after the PA, convolves it with the channel estimate and subtracts it from the received signal (1). The channel estimation is adjusted based on the achieved cancelation. The signal after analog canceler can be expressed with

$$y_{\mathrm{AC}}(t) = \left(h(t) - \hat{h}(t)\right) * x_{\mathrm{PA}}(t) + \sum_{i=1}^{K} s_i(t) + z(t), \quad (2)$$

where $\hat{h}(t)$ is the canceler response that estimates the channel. For more information on the canceler, please refer to [7].

After the analog-to-digital (AD) converter of the VST, further cancelation is done in the digital domain by utilizing a parallel-Hammerstein non-linearity to model the received self-interference signal

$$\hat{x}_{\mathrm{AC}}[n] = \sum_{\substack{m=1 \\ m \text{ odd}}}^{M} \hat{h}_{\mathrm{AC}}[n] * k_m[n] * |x[n]|^{m-1} x[n], \quad (3)$$

where M is the non-linearity order of the PA, $\hat{h}_{\mathrm{AC}}[n]$ is the estimated channel response for the residual SI after analog cancelation and $k_m[n]$ is the response of SI term of the mth order. Block least squares-based method is used to estimate the parameters.

A detailed explanation of the used method can be found in [6]. After digital cancelation, the remaining SI can be modeled with $x_{\mathrm{DC}}[n] = x_{\mathrm{AC}}[n] - \hat{x}_{\mathrm{AC}}[n]$, where $x_{\mathrm{AC}}[n]$ is the digitized version of $x_{\mathrm{AC}}(t) = \hat{h}_{\mathrm{AC}}(t) * x_{\mathrm{PA}}(t)$. The resulting signal with residual SI can be expressed with

$$y_{\mathrm{DC}}[n] = \sum_{i=1}^{K} s_i[n] + x_{\mathrm{DC}}[n] + z[n]. \quad (4)$$

If the cancelation has been sufficiently effective, the signals in $\sum_{i=1}^{K} s_i[n]$ can be detected if their power is stronger than the power of $x_{\mathrm{DC}}[n] + z[n]$.

After the digital cancelation has been performed and the subsequent residual SI power is as low as possible, interference-free detection of other signals becomes easier. In case of perfect SI cancelation, this is essentially the same as doing standard signal detection or spectral monitoring with a traditional half-duplex type receiver. Unfortunately, the cancelation might not always be sufficient and so we study how well signals other than the residual interference can be detected from measured signals with residual SI.

B. Signal Detection

The spectrum sensing is performed in two parts. In the first part, a recording of the signal is processed by means of a Fourier transform to obtain a time-frequency grid of N_f frequency elements and N_t time elements. The signal detection for a bin is based on the following hypotheses:

$$y_{\mathrm{DC}}[n] = \begin{cases} x_{\mathrm{DC}}[n] + z[n], & H_0 \\ s_i[n] + x_{\mathrm{DC}}[n] + z[n], & H_1 \end{cases} \quad (5)$$

where H_0 is the null hypothesis, there is no signal and H_1 is the alternative hypothesis, there is a signal from user i, who might be unknown. To determine the existence of signal s_i in a bin, we first define a binary function for each of the time-frequency bins as follows:

$$b^{(0)}_{(f,t)} = \begin{cases} 0, & P_{(f,t)} - P_{\mathrm{RX}} < \gamma \\ 1, & P_{(f,t)} - P_{\mathrm{RX}} \geq \gamma, \end{cases} \quad (6)$$

for all $f = 1, \ldots, N_f$ and $t = 1, \ldots, N_t$ bin frequency and time indices, respectively. Also, $P_{(f,t)}$ is the power measured in the bin corresponding to frequency f and time t, and γ is a threshold value set above the measured ground truth equivalent to the noise floor level P_{RX} at the receiver. Depending on the chosen threshold level γ, the produced binary table might contain a large number of false alarms caused by noise and residual self-interference.

In the second part, a rather simple reduction operation was performed to remove small concentrations of detections in the table. During operation, information of bins within the same region is combined in an iterative thresholding process to form decisions regarding to the presence or not of a signal. The combined information for the bins around (f,t) after iteration number $\upsilon = 1, 2, \ldots$, and considering a maximum distance R towards both lower and higher frequency and time indices, is

$$b^{(\upsilon)}_{(f,t)} = \begin{cases} 0, & \Psi^{(\upsilon)}_{N_f,N_t,R}(f,t) < \lambda \\ 1, & \Psi^{(\upsilon)}_{N_f,N_t,R}(f,t) \geq \lambda, \end{cases} \quad (7)$$

where $0 < \lambda < R^2$ is a thresholding value, and the iterative function is defined as

$$\Psi^{(\upsilon)}_{N_f,N_t,R}(f,t) = \sum_{\alpha=-\min\{N_f-f,R\}}^{\min\{f-1,R\}} \sum_{\beta=-\min\{N_t-t,R\}}^{\min\{t-1,R\}} b^{(\upsilon-1)}_{(f-\alpha,t-\beta)}. \quad (8)$$

Note that this function effectively counts the number of bins inside a square of size $2R+1$ and centered around (f,t), which have a value produced in previous iteration greater than the threshold level.

Last, the decision rule for bin (f,t) after Υ iterations is

$$b^{(\Upsilon)}_{(f,t)} = \begin{cases} 0 \Longrightarrow \text{decide } \mathcal{H}_0 \\ 1 \Longrightarrow \text{decide } \mathcal{H}_1. \end{cases} \quad (9)$$

III. Experimental Results and Analysis

The measurements were performed in the 2.4 GHz ISM band. In the performance measurements, the real transmit power of the waveforms was set to start at +23 dBm and then it was lowered with a 2 dB step size down to a maximum attenuation of 60 dB. The power difference before and after the cancelation stages were compared and the residual SI power

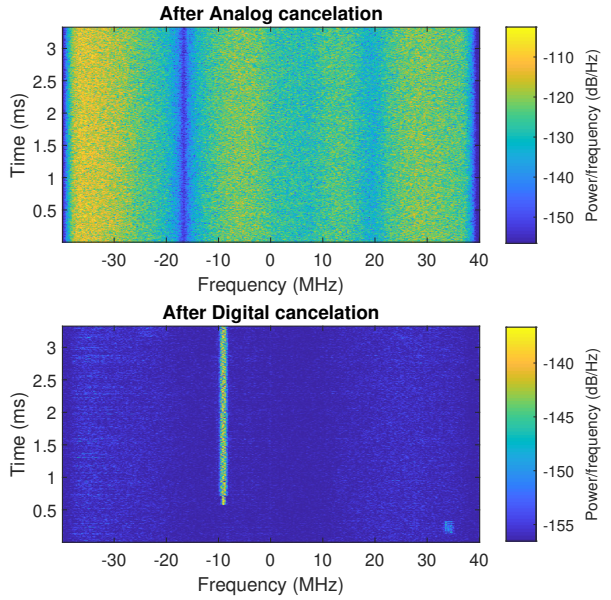

Fig. 4. Spectrograms demonstrating digital cancelation. The strong self-interference waveform is noise with a 80 MHz bandwidth, while the narrowband signals revealed after digital cancelation are signals from other users of the 2.4 GHz ISM-band.

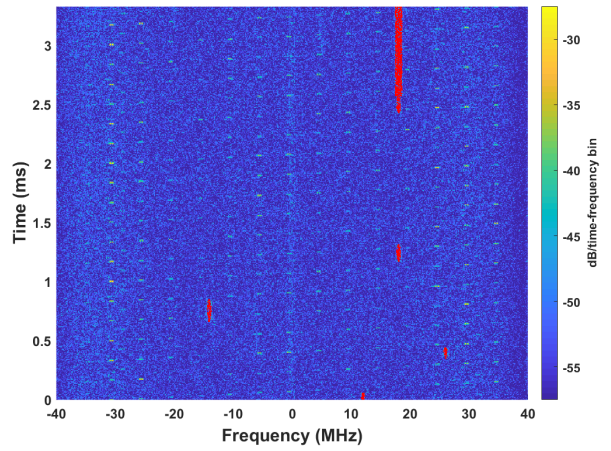

Fig. 5. Spectrogram demonstrating the detection result after digital cancelation for FH jamming waveform with detection threshold of 7 dB. Detected time-frequency bins are colored red. The used noise-reduction algorithm dismisses the detections caused by the residual self-interference, while still correctly marking the signals from the other users.

was calculated by comparing the signal power after digital cancelation to the known receiver 80 MHz noise floor, which was -73.5 dBm. Because of this, there is fluctuation in the digital cancelation performance and the residual SI power, which is caused by signals from the other users.

While the analog canceler is able to adjust its operation to give a better performance based on the measured cancelation even in a changing environment, during testing it was found that the estimation worked worse with some of the waveforms. To give good comparability between the different waveforms, the canceler was first calibrated with the 80 MHz bandwidth noise waveform and then the operation parameters were allowed to slowly adapt to the channel conditions during the measuring for all of the waveforms. This adaptation was turned off during the comparison measurement with different sweep frequencies for frequency hopping and triangular sweep waveforms. During these measurements, the initial calibration of the analog canceler was done like before using the 80 MHz noise signal and then the update function was turned off.

The analog settings were fixed for all of the FH and triangular sweep measurements to ensure that the canceler performance does not drift between measurement runs. The transmit power was fixed at 13 dBm to ensure good analog and digital cancelation performance while still allowing some residual SI after the digital cancelation so that it remains the dominant signal component and masks other random signals in the channel. The measured sweep frequencies were 1-60 kHz with 5 kHz steps for both of the waveforms.

In all measurements, the reference level of the AD converter was set 10 dB higher than the received signal power and it was adjusted accordingly when the TX power was changed. This limit slightly reduced the optimal performance of some waveforms with a lower peak-to-average power ratio, but it was deemed necessary to maintain their comparability.

The recorded channel was not isolated from public transmissions, which unfortunately produced some ambiguity in the cancelation performance results. However, recording a noisy channel was crucial for our secondary objective of spectral monitoring. The rather dramatic effect in SI cancelation of the transmitted jamming waveform can be seen from Fig. 4, where the two narrowband signals from other users are completely masked by the wideband SI after analog cancelation, however they become clearly visible after digital cancelation.

A visual representation of signal detection can be seen from Fig. 5. In the figure, the detected time-frequency bins have been highlighted with red color over a spectrogram of the whole signal. The waveform used in the figure was FH tones at GFSK spacing, with a sweep frequency of 6 kHz. The detection threshold was set to 7 dB. The figure demonstrates how the noise reduction algorithm removes the false detections that should be caused by the rather strong residual SI. In all of the measurements the noise reduction algorithm presented before with (7) and (8) was operated with a detection range of $R = 5$ and the percentage of positive detections was $\lambda = 1/3$. The number of iterations was $\Upsilon = 3$. All iterations were performed with the same R and λ values.

During detection processing, the ground truth was created manually for all the received signals and the detection performance was calculated from the detection result tables obtained from running the detection algorithm at various different threshold levels. These results were compared automatically against the ground truth to obtain the percentages of detected signals and false alarms, both of which had a resolution of one time-frequency bin. The transmit power was set at 7 dBm to ensure some self-interference was left after digital cancelation.

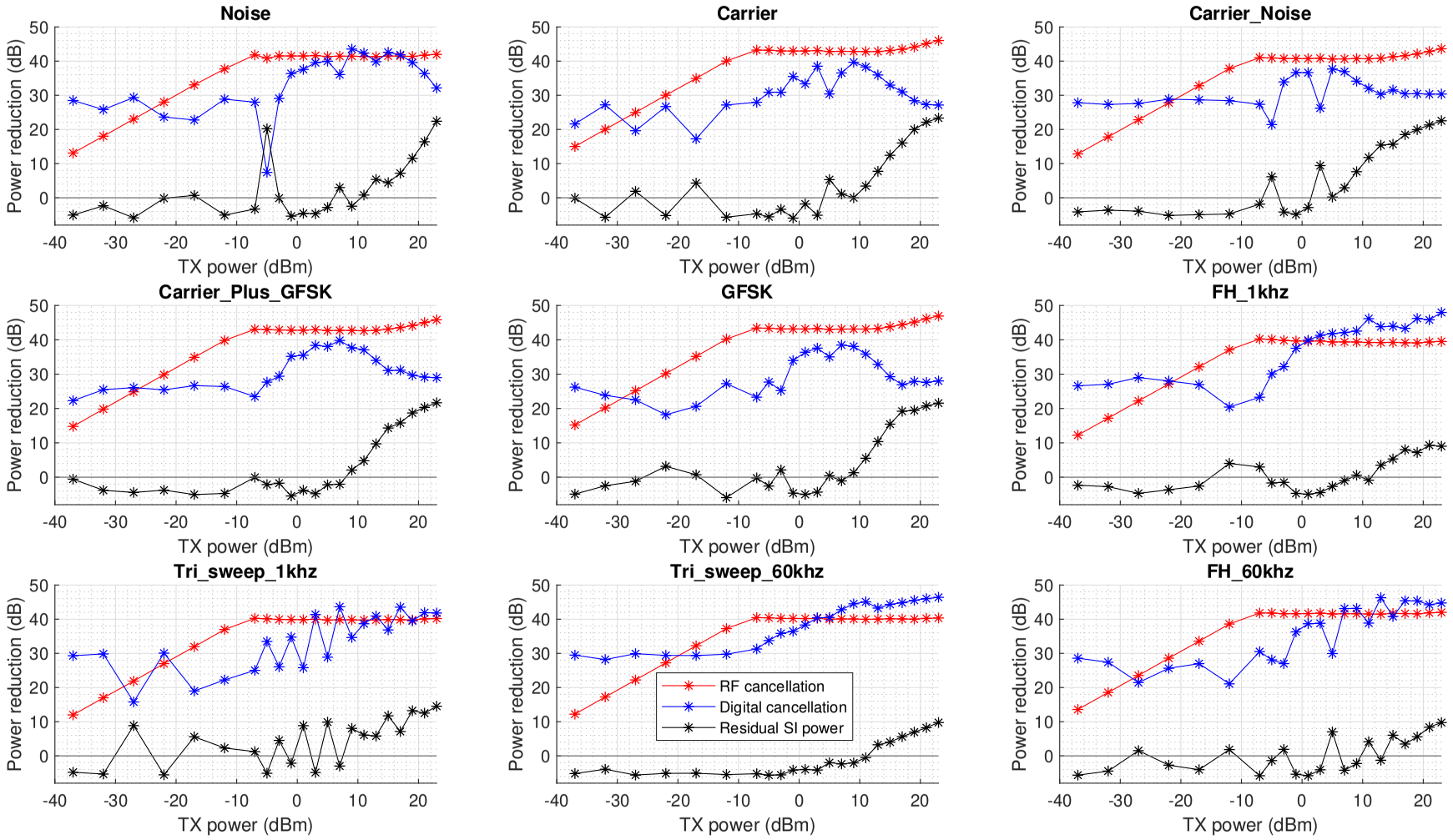

Fig. 6. Cancelation performance of the jamming waveforms at different TX transmit powers.

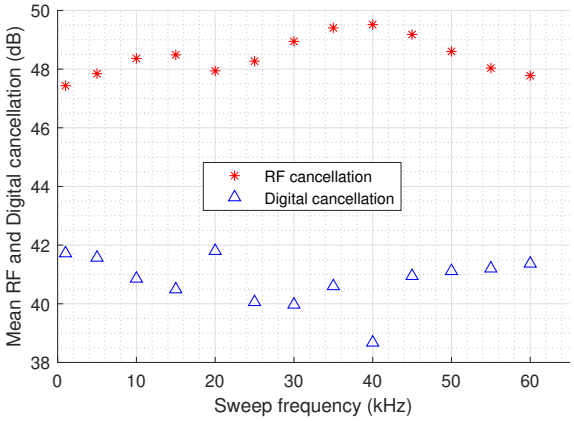

Fig. 7. Cancelation performance of FH signal at different sweep frequencies.

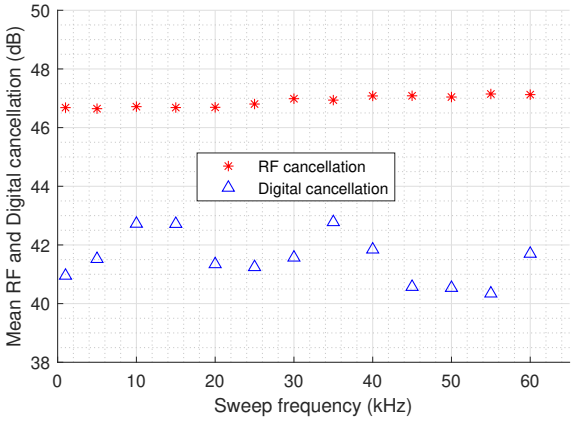

Fig. 8. Cancelation performance of triangular sweep signal at different sweep frequencies.

A. *Self-interference Cancelation*

Fig. 6 shows the RF- and digital cancelation performance of the chosen jamming waveforms and the residual SI remaining after the cancelation at different transmit power levels. The total signal power level was calculated after every cancelation stage. The RF cancelation performance is rather similar for all of the chosen signals. This stage achieved a cancelation of at least 40 dB for all of the signals above transmit powers of -10 dBm. In this paper, the RF cancelation is a combination of the circulator isolation, which was 20 dB, and the analog canceler. The analog canceler was first calibrated with the 80 MHz noise signal, after which the automatic adjustment was allowed to change the parameters of the canceler during the rest of the measurements. Therefore, the minor differences between the waveforms can be explained by how well the analog canceler could follow the channel dynamics when using a certain waveform, as well as by whether the canceler happened to have a strong attenuation at the frequencies occupied by a specific waveform.

The analog cancelation performance was not constant for the whole 80 MHz band, as can be seen from the upper spectrogram in Fig. 4. There are clearly visible frequencies of stronger and weaker cancelation. These differences in SI power are passed to the following digital cancelation stage, where the canceler might not be able to effectively reduce the SI from the entire band. This effect is likewise visible in the lower spectrogram of Fig. 4. A further observation is that the RF cancelation performance seems to decrease when the transmit power is lowered. This is caused by the inability of the analog canceler to properly estimate the channel parameter $\hat{h}(t)$ of the cancelation signal, which ends up causing additional interference in the lowest transmit powers.

The digital cancelation shows more variability when comparing the chosen waveforms. Overall this stage appears to give a performance of at least 20 dB apart from the two fluctuations in 1 kHz triangular sweep and noise plots, which are most likely caused by signals from other users. The region of optimal cancelation due to the transmitted power appears to be at different power levels for the waveforms. This is important to know if it is desirable to change the waveform during operation, since the transmit power might need to be adjusted to ensure good operation of FD functionality. Of course, to ensure good FD operation, the residual power after cancelation should be as close to the noise floor as possible, regardless of the optimal performance region of TX power level. It follows that although the cancelation performance of the sweeping signals seems to improve with a higher TX power, the residual SI power left after the cancelation is also increasing over the noise floor, which means that low powered signals of interest can no longer be received or even spotted.

The effect of changing the sweeping frequency can be seen from Figs. 7 and 8. The sweep frequency does not seem to have a strong effect on the analog cancelation of either of the waveforms. In the frequency hopping case there is a slight increase of about 1 dB in the analog cancelation when the sweep frequency is increased from 1 to 60 kHz. With the triangular sweep, the analog cancelation performance fluctuates between 47 and 50 dB. This effect might be caused by minor changes in the channel.

The digital cancelation performance seems to move randomly around a mean value of 41 dB for FH and 42 dB for the triangular waveform. This fluctuation can be again explained by the power calculation method used on a noisy channel. If there happened to be strong signals in the channel during the measurement, the digital cancelation performance shows a worse result than if there were no other users.

From the obtained results it can be deduced that the sweep frequency does not seem to affect the SI cancelation, at least if the analog canceler has been precalibrated and the automatic adjustment is disabled. As was shown in our previous paper [16], the sweep frequency has an effect on the performance of jamming, so it is reassuring to know that this parameter does not have a major effect on FD operation.

B. *Detection Performance*

Next we will look at the results obtained from signal detection and false alarms for the waveforms at different detection

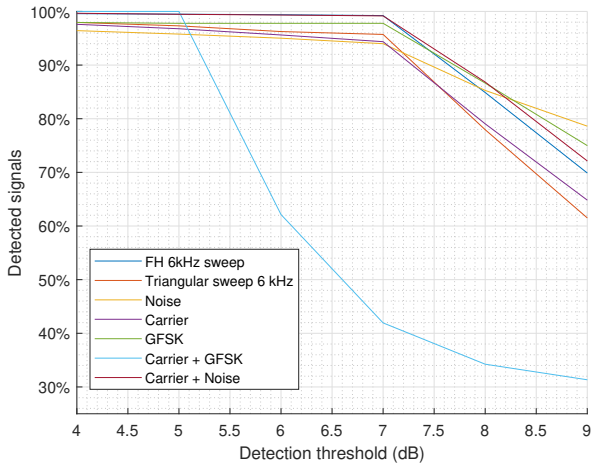

Fig. 9. Detection results of waveforms at different detection thresholds. Result of "Carrier + GFSK" waveform was caused by a weak WLAN signal that was spectrally large compared to other signals.

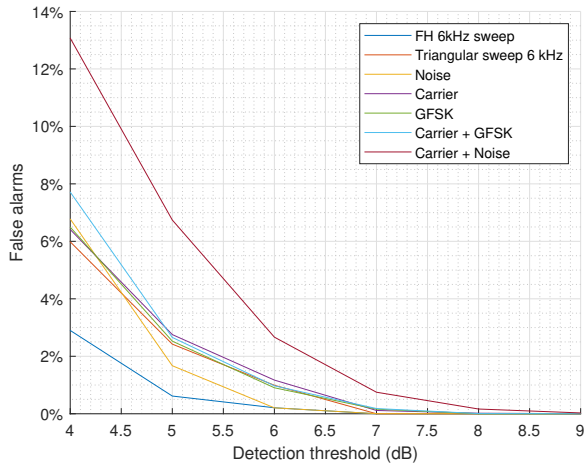

Fig. 10. False alarms of waveforms at different detection thresholds.

thresholds. The detection results can be seen from Fig. 9. In the figure we can see that none of the chosen waveforms particularly affects the detection performance, apart from the large difference with the "Carrier + GFSK" waveform. This anomaly was caused by a weak WLAN signal which was flagged for the ground truth, but which was detected by the algorithm at a relatively low threshold. Overall, the results in the figure are not well comparable between each other, since the measured channel was not isolated and the number, protocol and power of the signals transmitted by other users were not consistent. It is possible that a certain TX waveform might cause the cancelation operations to more strongly attenuate the signals we would like to detect. To see if the chosen waveform causes a noticeable difference in the detection, a more rigorous measurement campaign should be performed in a controlled environment. This is however outside the scope of this paper.

The number of false alarms presented in Fig. 10 at different detection thresholds shows how the detection algorithm used is able to deal with the residual interference left after SI cancelation. The frequency hopping waveform seems to have the best detection performance in the presence of SI, since there are no false alarms at threshold of 7 dB even though there are strong residual SI signals visible in Fig. 5. Triangular sweep was likewise able to give a rather good false alarm performance even though the residual SI was quite strong. During testing, this increase in performance was found to be caused by the time-frequency profile of the SI from these waveforms being relatively small, which is why the noise reduction operation was able to remove them from the detection table. Meanwhile the SI from the rest of the signals was a whole measurement length interfering signal at different frequencies. The noise reduction algorithm was not able to discern these signals from the signals we actually wanted to detect. The 500 kHz noise at carrier frequencies performed the worst, which is intuitive based on previous observations.

The detection performance could be further improved by tailoring the algorithm to optimally remove the self-interference while preserving the detections from the signals of interest. During testing an alternative initial detection algorithm was conceived, where the local mean power was calculated for a subtable of time-frequency bins with a width of a few frequencies and length of a whole measurement. The power of the individual bins in the subtable were then compared against the threshold over this local mean. This algorithm was actually giving extremely good performance for all of the chosen waveforms, but unfortunately it was found that it also decreased the detection of WLAN signals, since they were usually in bursts with a period that is at least half of the measurement period. Therefore, since it was deemed more important to preserve the detection of WLAN signals than improve false alarm probability at low detection thresholds, a more traditional detection algorithm was used instead.

IV. Conclusion

In this paper, an experimental full-duplex capable transceiver was presented and its self-interference cancelation performance was measured for various typical jamming waveforms. The sum of antenna and analog canceler cancelation was round 40 dB for all of the waveforms, while the digital cancelation achieved self-interference mitigation of 20–45 dB, depending on the transmit power and waveform. Additionally, the signal detection of other users of the radio channel was studied over samples with imperfect self-interference cancelation. The study found that wide-band waveforms, which in this case meant wideband noise and sweeping signals, typically achieve better cancelation and signal detection.

References

[1] E. Bond, B. Crowther, and B. Parslew, "The rise of high-performance multi-rotor unmanned aerial vehicles - how worried should we be?" in *Proc. Workshop on Research, Education and Development of Unmanned Aerial Systems*, Nov. 2019.

[2] K. Pärlin, M. M. Alam, and Y. Le Moullec, "Jamming of UAV remote control systems using software defined radio," in *Proc. International Conference on Military Communications and Information Systems*, Jun. 2018.

[3] K. Pelechrinis, M. Iliofotou, and S. V. Krishnamurthy, "Denial of service attacks in wireless networks: The case of jammers," *IEEE Communications Surveys & Tutorials*, vol. 13, no. 2, pp. 245–257, May 2011.

[4] M. Lichtman, J. D. Poston, S. Amuru, C. Shahriar, T. C. Clancy, R. M. Buehrer, and J. H. Reed, "A communications jamming taxonomy," *IEEE Security & Privacy*, vol. 14, no. 1, pp. 47–54, Feb. 2016.

[5] K. E. Kolodziej, B. T. Perry, and J. S. Herd, "In-band full-duplex technology: Techniques and systems survey," *IEEE Transactions on Microwave Theory and Techniques*, vol. 67, no. 7, pp. 3025–3041, Feb. 2019.

[6] D. Korpi, M. Heino, C. Icheln, K. Haneda, and M. Valkama, "Compact inband full-duplex relays with beyond 100 dB self-interference suppression: Enabling techniques and field measurements," *IEEE Transactions on Antennas and Propagation*, vol. 65, no. 2, pp. 960–965, Nov. 2017.

[7] J. Tamminen, M. Turunen, D. Korpi, T. Huusari, Y. Choi, S. Talwar, and M. Valkama, "Digitally-controlled RF self-interference canceller for full-duplex radios," in *Proc. 24th European Signal Processing Conference*, Aug. 2016.

[8] T. Riihonen, D. Korpi, M. Turunen, and M. Valkama, "Full-duplex radio technology for simultaneously detecting and preventing improvised explosive device activation," in *Proc. International Conference on Military Communications and Information Systems*, Jun. 2018.

[9] T. Riihonen, D. Korpi, M. Turunen, T. Peltola, J. Saikanmäki, M. Valkama, and R. Wichman, "Military full-duplex radio shield for protection against adversary receivers," in *Proc. International Conference on Military Communications and Information Systems*, May 2019.

[10] J. Saikanmäki, M. Turunen, M. Mäenpää, A. Saarinen, and T. Riihonen, "Simultaneous jamming and RC system detection by using full-duplex radio technology," in *Proc. International Conference on Military Communications and Information Systems*, Sep. 2019.

[11] C. Baquero Barneto, T. Riihonen, M. Turunen, L. Anttila, M. Fleischer, K. Stadius, J. Ryynänen, and M. Valkama, "Full-duplex OFDM radar with LTE and 5G NR waveforms: Challenges, solutions, and measurements," *IEEE Transactions on Microwave Theory and Techniques*, vol. 67, no. 10, pp. 4042–4054, Aug. 2019.

[12] A. Mpitziopoulos, D. Gavalas, C. Konstantopoulos, and G. Pantziou, "A survey on jamming attacks and countermeasures in WSNs," *IEEE Communications Surveys & Tutorials*, vol. 11, no. 4, pp. 42–56, Dec. 2009.

[13] D. Borio, C. O'Driscoll, and J. Fortuny, "Fast and flexible: Tracking and mitigating a jamming signal with an adaptive notch filter," *Inside GNSS*, vol. 9, pp. 67–73, Mar. 2014.

[14] K. Pärlin, T. Riihonen, and M. Turunen, "Sweep jamming mitigation using adaptive filtering for detecting frequency agile systems," in *Proc. International Conference on Military Communications and Information Systems*, May 2019.

[15] B. Van den Bergh and S. Pollin, "Keeping UAVs under control during GPS jamming," *IEEE Systems Journal*, vol. 13, no. 2, pp. 2010–2021, Dec. 2018.

[16] J. Marin, M. Heino, J. Saikanmäki, M. Mäenpää, A. P. Saarinen, and T. Riihonen, "Perfecting jamming signals against RC systems: An experimental case study on FHSS with GFSK," in *Proc. IEEE 31st Annual International Symposium on Personal, Indoor and Mobile Radio Communications*, Oct. 2020.

[17] M. Vuorenmaa, J. Marin, M. Heino, M. Turunen, and T. Riihonen, "Radio-frequency control and video signal recordings of drones," Nov. 2020. [Online]. Available: https://doi.org/10.5281/zenodo.4264467

[18] V. Chamola, P. Kotesh, A. Agarwal, Naren, N. Gupta, and M. Guizani, "A comprehensive review of unmanned aerial vehicle attacks and neutralization techniques," *Ad Hoc Networks*, vol. 111, p. 102324, 2021.